Breast ultrasound waveform tomography: Using both transmission and reflection data, and numerical virtual point sources

Lianjie Huang[a], Youzuo Lin[a], Zhigang Zhang[a], Yassin Labyed[a], Sirui Tan[a], Nghia Nguyen[a], Kenneth Hanson[a], Daniel Sandoval[b], and Michael Williamson[b]

[a]Los Alamos National Laboratory, Los Alamos, NM 87545, USA;
[b]University of New Mexico, Department of Radiology, Albuquerque, NM 87131, USA

ABSTRACT

Ultrasound transmission tomography usually generates low-resolution breast images. We improve sound-speed reconstructions using ultrasound waveform tomography with both transmission and reflection data. We validate the improvement using computer-generated synthetic-aperture ultrasound transmission and reflection data for numerical breast phantoms. Our tomography results demonstrate that using both transmission and reflection data in ultrasound waveform tomography greatly enhances the resolution and accuracy of tomographic reconstructions compared to ultrasound waveform tomography using either transmission data or reflection data alone. To verify the capability of our novel ultrasound waveform tomography, we design and manufacture a new synthetic-aperture breast ultrasound tomography system with two parallel transducer arrays for clinical studies. The distance of the two transducer arrays is adjustable for accommodating different sizes of the breast. The parallel transducer arrays also allow us to easily scan the axillary region to evaluate the status of axillary lymph nodes and detect breast cancer in the axillary region. However, synthetic-aperture ultrasound reflection data acquired by firing each transducer element sequentially are usually much weaker than transmission data, and have much lower signal-to-noise ratios than the latter. We develop a numerical virtual-point-source method to enhance ultrasound reflection data using synthetic-aperture ultrasound data acquired by firing each transducer element sequentially. Synthetic-aperture ultrasound reflection data for a breast phantom obtained using our numerical virtual-point-source method reveals many coherent ultrasound reflection waveforms that are weak or invisible in the original synthetic-aperture ultrasound data. Ultrasound waveform tomography using both transmission and reflection data together with numerical virtual-point-source method has great potential to produce high-resolution tomographic reconstructions in clinical studies of breast ultrasound tomography.

Keywords: Breast cancer, numerical virtual point source, reflection, transmission, synthetic-aperture ultrasound, ultrasound ray tomography, ultrasound tomography, ultrasound waveform tomography, virtual point source.

1. INTRODUCTION

Synthetic-aperture ultrasound is a promising imaging modality for improving medical ultrasound imaging.[1–26] It has been recently used for ultrasound tomography (UST). UST has great potential to provide quantitative estimations of mechanical properties of breast tumors for accurate detection and characterization of breast cancers. Ultrasound ray tomography (USRT) reconstructs the sound-speed and ultrasound attenuation distributions within the breast.[27–36] One of the primary advantages of USRT is its computational efficiency. However, USRT can only produce low-resolution images, and could fail to image highly heterogeneous, dense breasts. With the increasing computing power, ultrasound waveform tomography (USWT) is becoming feasible.[37–41] Ultrasound waveform tomography has the following advantages: (1) USWT could generate higher-resolution breast images than those obtained with ultrasound ray tomography; (2) USWT properly handles complex wave phenomena in heterogeneous, dense breasts; (3) USWT could accurately reconstruct mechanical properties of small breast tumors; and (4) USWT has the potential to image spiculated features of breast tumors.

Ultrasound tomography often uses only transmission data. Ultrasound transmission data from the breast are much simpler than reflection data, particularly for dense breasts. However, ultrasound tomography using only transmission data usually produces low-resolution images. Ultrasound reflection data carry rich information about the breast, and ultrasound reflection imaging often generates high-resolution images.

Send correspondence to Lianjie Huang: ljh@lanl.gov

Medical Imaging 2014: Ultrasonic Imaging and Tomography, edited by Johan G. Bosch, Marvin M. Doyley, Proc. of SPIE Vol. 9040, 90400T · © 2014 SPIE
CCC code: 1605-7422/14/$18 · doi: 10.1117/12.2043136

We employ both transmission and reflection data for ultrasound waveform tomography. We use noisy-free, numerical phantom data to demonstrate that combining ultrasound transmission data with reflection data for USWT greatly improves image resolution and the accuracy of sound-speed reconstructions.

For imaging soft tissues, ultrasound reflection data acquired using synthetic-aperture ultrasound by firing each element sequentially have much lower signal-to-noise ratios than those of ultrasound transmission data. This is partially because of weak signals emitting from a single element of a transducer array, ultrasound attenuation in soft tissues, and week scattering/reflection from heterogeneities in soft tissues.

Virtual sources have been introduced into synthetic-aperture ultrasound to improve signal-to-noise ratios of ultrasound reflection data.[42–44] In synthetic-aperture ultrasound with virtual sources, a number of transducer elements are fired with a different delay time for each element to form an ultrasound wave emitting from a virtual source. The virtual source can be located at any spatial location near a transducer array, on the transducer surface, or behind the transducer array, or in the front side of the transducer array. For breast imaging, it is not suitable to form virtual point sources in the front side of transducer arrays to avoid potential harms of heat generated by ultrasound focusing.

We use our ultrasound tomography system with two parallel transducer arrays to explore the use of virtual sources for ultrasound tomography. Our transducer arrays have a total of 768 transducer elements. The distance of these two arrays is adjustable for scanning different sizes of the breast. Imaging axillary lymph nodes can provide the single most important prognostic information for patients with primary breast cancer.[45] The parallel transducer arrays in our breast ultrasound tomography system allow us to easily scan the axillary region for imaging and characterizing axillary lymph nodes and detecting beast cancer in the axillary region. In our ultrasound tomography system, the transducer arrays are translated vertically to scan the breast from the chest wall/axillary region to the nipple region to acquire ultrasound transmission and reflection data for whole-breast ultrasound tomography.

To enhance ultrasound reflection data, we develop a numerical virtual-point-source method to combine synthetic-aperture ultrasound data acquired with a breast ultrasound tomography system. We use this method and a breast phantom to generate ultrasound reflection data for numerical virtual point sources, and compare them with those acquired using our breast ultrasound tomography system. Ultrasound reflection data with numerical virtual point sources unmask many coherent reflection waveforms that are very weak or invisible in the original synthetic-aperture ultrasound data and those acquired with virtual sources. Signal-to-noise ratios of the new data are much higher than the other data. Ultrasound waveform tomography with these high-quality numerical-virtual-source data would significantly boost the capability of ultrasound waveform tomography for accurate characterization of breast cancer.

2. ULTRASOUND WAVEFORM TOMOGRAPHY WITH BOTH TRANSMISSION AND REFLECTION DATA

We first study how ultrasound reflection data can improve ultrasound waveform tomography. USWT iteratively solves a minimization problem[40,41]

$$E(\mathbf{m}) = \min_{\mathbf{m}} \left\{ \sum_{i_s=1}^{N} \sum_{i_r=1}^{N} \int [d(t,i_r,i_s) - p(t,i_r,i_s,)]^2 dt + \lambda \, \mathrm{R}(\mathbf{m}) \right\}, \tag{1}$$

where $E(\mathbf{m})$ is the misfit function, d is an ultrasound waveform acquired at transducer element i_r and emitted from transducer element i_s, N is the total number of transducer elements to transmit/receive ultrasound waveforms, λ is a relaxation parameter, R is a regularization term, and $\mathbf{m}$ is the model parameter given by

$$\mathbf{m} = \begin{bmatrix} V \text{ or } K \\ \rho \end{bmatrix}, \tag{2}$$

where $V = \sqrt{K/\rho}$ is the sound speed, $K(\mathbf{r})$ is the bulk modulus, $\rho(\mathbf{r})$ is the density, and these parameters are all functions of spatial location $\mathbf{r}$. In equation (1), p is a computer-generated (synthetic) ultrasound waveform for transmitting element i_s, and is a function of the model parameter $\mathbf{m}$. The first team on the right side of equation (1) is a data misfit term, and the second one is a regularization term. We use USWT with a modified total-variation regularization scheme[40] for this study.

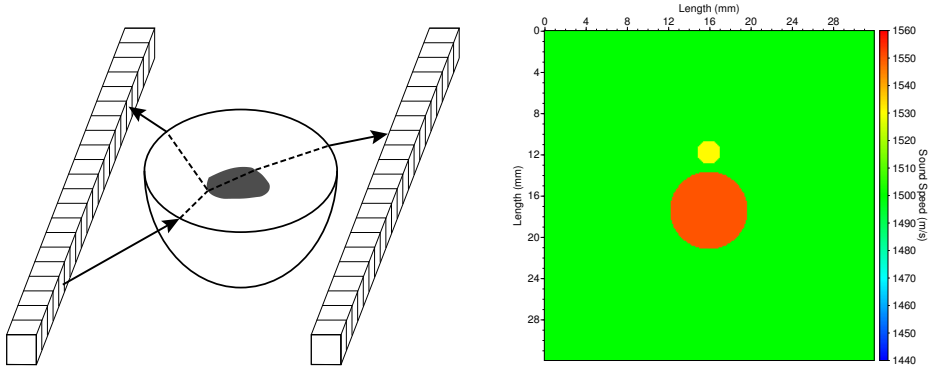

(a) Two parallel transducer arrays

(b) Numerical breast phantom with two small tumors

Figure 1: Illustration of two parallel transducer arrays in (a) with a total of 768 elements for synthetic-aperture ultrasound tomography, together with a numerical breast phantom in (b) scanned with the parallel transducer arrays in (a).

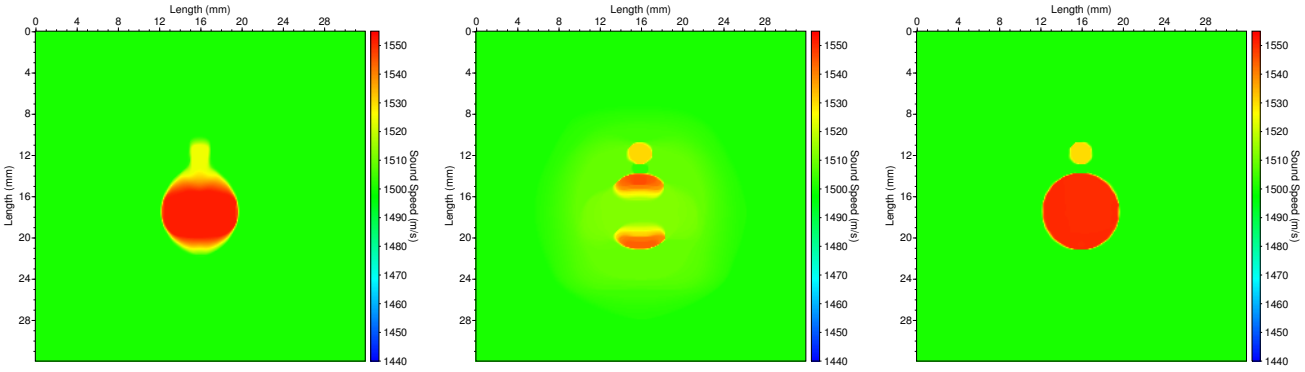

(a) USWT with only transmission data

(b) USWT with only reflection data

(c) USWT with both transmission and reflection data

Figure 2: A numerical breast phantom with two small tumors in Fig. 1(a) is reconstructed using ultrasound waveform tomography with (a) transmission data only, (b) reflection data only, and (c) both transmission and reflection data. USWT reconstruction result in (c) is much better than those in (a) and (b).

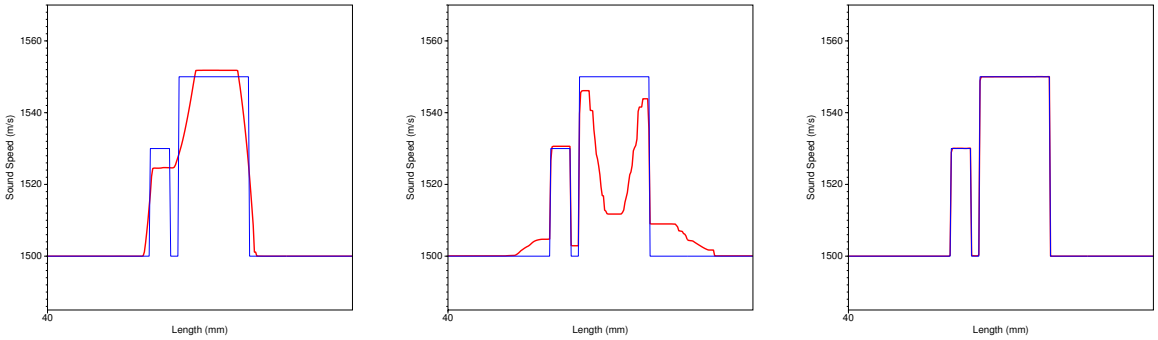

(a) A vertical profile in red of Fig. 2(a)

(b) A vertical profile in red of Fig. 2(b)

(c) A vertical profile in red of Fig. 2(c)

Figure 3: Comparison of vertical profiles (in red) of USWT sound-speed reconstruction results in Fig. 2 along the centers of the two tumors with the correct profile (in blue) of the numerical phantom in Fig. 1(b).

We compute synthetic waveforms p in equation (1) using a time-domain, high-order-accurate finite-difference scheme to solve the acoustic-wave equation

$$\left[\frac{1}{K(\mathbf{r})}\frac{\partial^2}{\partial t^2} - \nabla\cdot\left(\frac{1}{\rho(\mathbf{r})}\nabla\right)\right] p(t,\mathbf{r}) = S(t)\delta(\mathbf{r}-\mathbf{r}_0), \tag{3}$$

where $S(t)$ is the source waveform, $\mathbf{r}_0$ is the location of a transmitting element, and $p(\mathbf{r},t)$ is the pressure wavefield, or ultrasound waveform.

The goal of USWT is to reconstructs physical properties such as the sound speed, density, and attenuation, so that synthetic (computer-generated) ultrasound waveforms optimally fit entire acquired ultrasound waveforms, which can be ultrasound transmission data, or reflection data, or both. We use numerical phantom data to study the capability of sound-speed reconstructions using USWT with only transmission data, or only reflection data, or with both transmission and reflection data.

We generate synthetic ultrasound transmission and reflection data for an ultrasound tomography system with two parallel transducer arrays as shown in Fig. 1(a) to scan a numerical breast phantom in Fig. 1(b). The numerical phantom contains two small tumors: one with a diameter of 2 mm, and the other with a diameter of 8 mm. The two parallel transducer arrays are placed at the top and bottom sides of the numerical phantom. The center frequency of synthetic ultrasound data is 1 MHz. We conduct sound-speed reconstructions using our ultrasound waveform tomography algorithm with a modified total-variation regularization scheme.[40] Figure. 2(a) displays the USWT result obtained using only the transmission data. The images of the two tumors cannot be separated. Figure. 2(b) shows our USWT result produced using only the reflection data. The images of the two small tumors are no longer connected to each other. However, USWT with only the reflection data cannot fully reconstruct the 8-mm tumor. Finally, we conduct USWT using both transmission and reflection data together, and obtain almost perfect reconstructions of the two small tumors, as shown in Fig. 2(c). Fig. 3 shows a comparison of velocity profiles of USWT reconstructions in Fig. 2 with the exact values. This numerical example demonstrates that ultrasound waveform tomography with both transmission and reflection data greatly improves sound-speed reconstructions compared to USWT using either transmission data or reflection data alone.

In our numerical implementation, we first conduct ultrasound waveform tomography with transmission data to generated a low-resolution image, and then carry out USWT with both transmission and reflection data to produce high-resolution tomographic reconstruction results. This is a multi-scale approach to ultrasound waveform tomography.

In the next example, we conduct ultrasound waveform tomography for a numerical breast phantom containing a small spiculated cancer in a random medium mimicking the heterogeneous breast tissue (Fig. 4a). The size of the central part

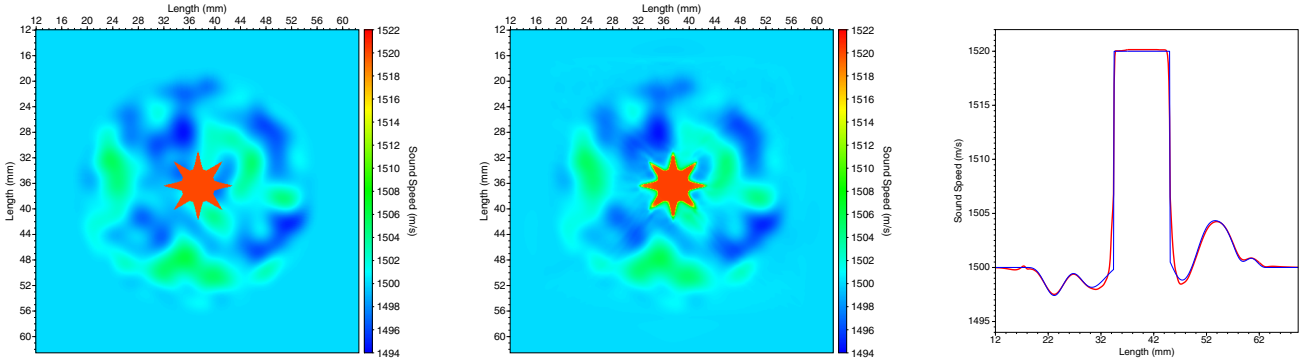

(a) Numerical breast phantom containing a spiculated cancer in a random background tissue

(b) Ultrasound waveform tomography with both transmission and reflection data

(c) Comparison between a vertical profile in (b) and the correct one in (a)

Figure 4: Ultrasound waveform tomography for a numerical breast phantom in (a) containing a spiculated cancer in a random medium gives an accurate reconstruction in (b) when using both transmission and reflection data. A comparison in (c) between a vertical sound-speed profile along the center of the spiculated cancer of USWT reconstruction result in (b) with the correct profile of (a) shows accurate sound-speed reconstruction. The reconstruction result is in red in (c), and the correct one is in blue.

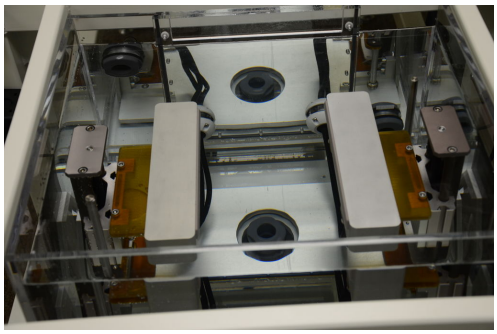

(a) Parallel transducer arrays in LANL's prototype for clinical breast ultrasound tomography

(b) A breast phantom with many inclusions

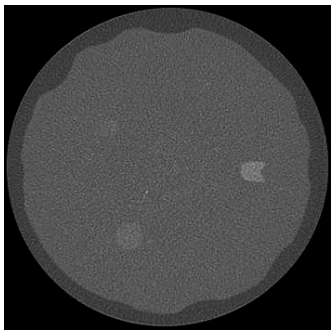

(c) An X-ray CT slice of the breast phantom in (b)

Figure 5: Our newly custom-built synthetic-aperture breast ultrasound tomography system with two parallel transducer arrays and a total of 768 transmitting/receiving elements (a), is used to scan a breast phantom in (b) containing many different inclusions as shown in an X-ray CT slice in (c).

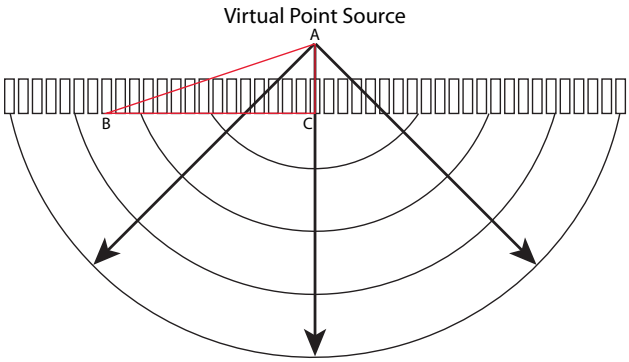

(a) An ultrasound virtual point source behind a transducer array

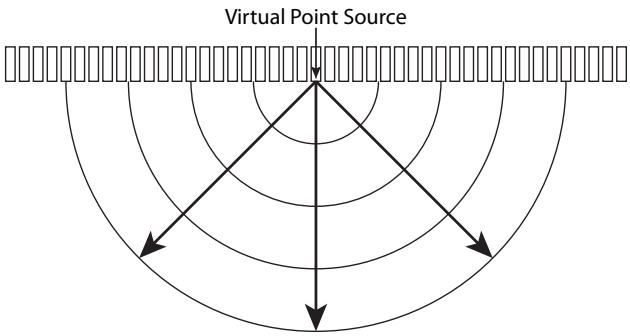

(b) An ultrasound virtual point source on the surface of a transducer array

Figure 6: Ultrasound virtual point sources can be formed either (a) behind a transducer array or (b) on the surface of a transducer array. For breast imaging, it is not suitable to form a virtual point source in the front side of a transducer array to avoid potential harms of heat generated by ultrasound focusing.

of the spiculated cancer (not including the spiculated feature) is 6 mm. The distances between the tips of the spiculated features and the center of the cancer are all 9 mm. USWT with both transmission and reflection data accurately reconstructs the random background tissue, the spiculated cancer, and the spiculated features, as shown in Fig. 4(b). Fig. 4(c) is a comparison of two vertical profiles in Figs. 4(a) and (b) along the center of the cancer, and confirms that our USWT produces accurate sound-speed values of the spiculated cancer and the surrounding tissue. Note that the vertical profiles cut through two tips of the spiculated features in the vertical direction in Figs. 4(a) and (b).

3. VIRTUAL POINT SOURCES FOR BREAST ULTRASOUND TOMOGRAPHY

Ultrasound reflection signals from soft tissues acquired using synthetic-aperture ultrasound by firing each element sequentially are much weaker and have much lower signal-to-noise ratios than ultrasound transmission signals.

Because of the potential significant improvement of breast ultrasound tomography when incorporating ultrasound reflection data, we explore the use of virtual point sources to enhance signal-to-noise ratios of ultrasound reflection signals. We first implement virtual point sources on ultrasound transducer arrays of our synthetic-aperture breast ultrasound tomography system. We then develop a numerical virtual-point-source method to implement virtual point sources on acquired synthetic-aperture ultrasound data.

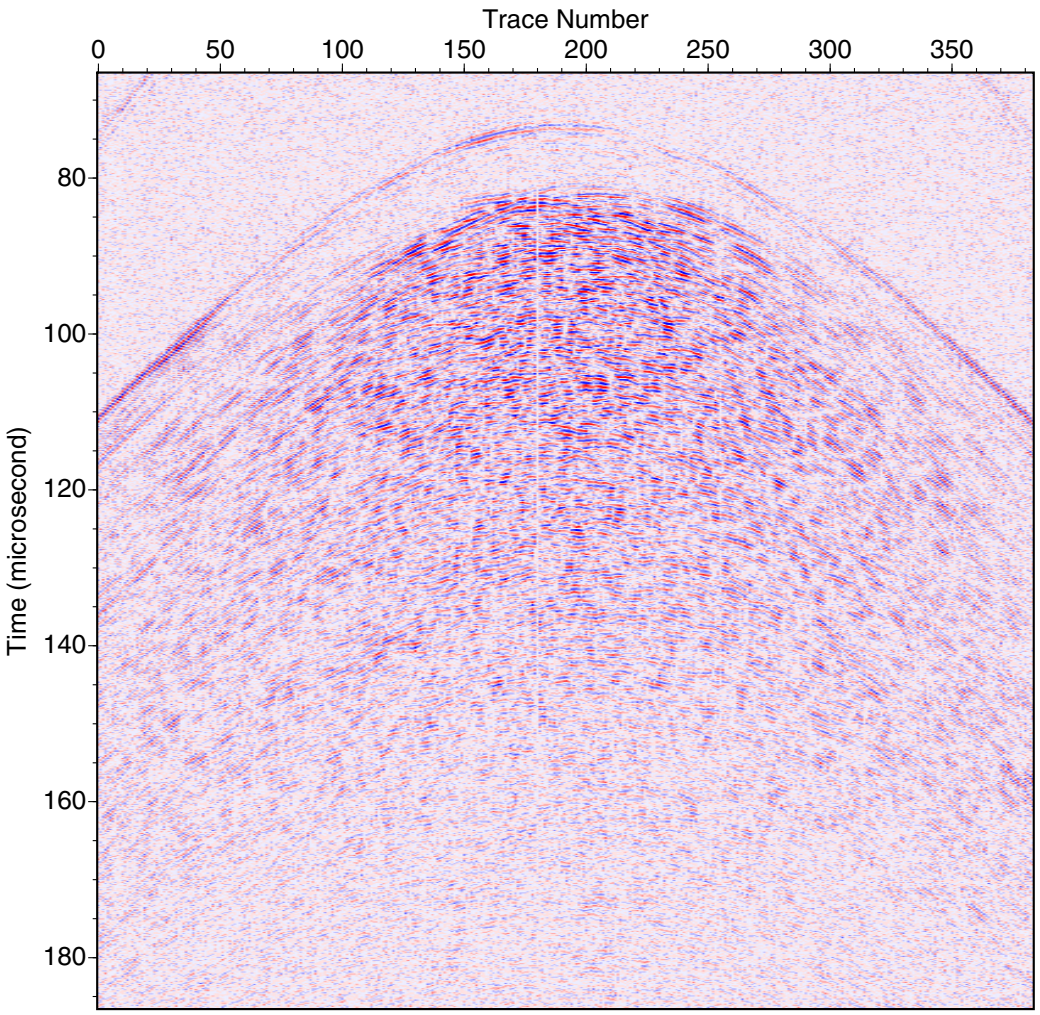

Figure 7: Synthetic-aperture ultrasound reflection data from the breast phantom in Fig. 5(b) acquired by firing each single element sequentially. The transmitting element is No. 192 near the center of a transducer array. Data on two dead/weak transducer elements are shown as two vertical white strips.

3.1 Implementing virtual point sources on transducers

We have designed and manufactured a clinical breast ultrasound tomography prototype with two parallel transducer arrays (Fig. 5a). Each transducer array consists of 384 elements. The two transducer arrays scan the breast in a warm water tank. The distance of the two transducer arrays is adjustable to accommodate different sizes of the breast. The two parallel transducer arrays are easily to place one of them under the arm to scan the axillary region. The transducer arrays are translated vertically to scan the breast from the chest wall/axillary region to the nipple region to acquire synthetic-aperture ultrasound transmission and reflection data for whole-breast ultrasound tomography. It takes two to three minutes to scan a breast. The University of New Mexico Hospital conducts *in vivo* patient studies using this breast ultrasound tomography system from Los Alamos National Laboratory (LANL).

We use our breast ultrasound tomography system to scan a breast phantom shown in Fig. 5(b). The phantom contains 12 different mass/cyst inclusions and a number of calcifications in different locations. The sizes of the mass/cyst inclusions range from 4 mm to 12 mm. The solid-mass inclusions embedded in the glandular material mimic fibroadenoma and cancer, including spiculated cancer. Fig. 5(c) is a X-ray CT slice of the phantom showing a cyst, two solid-mass inclusions, and a calcification.

We estimate the sound-speed of water c_w using either tomography of ultrasound data when scanning water only, or

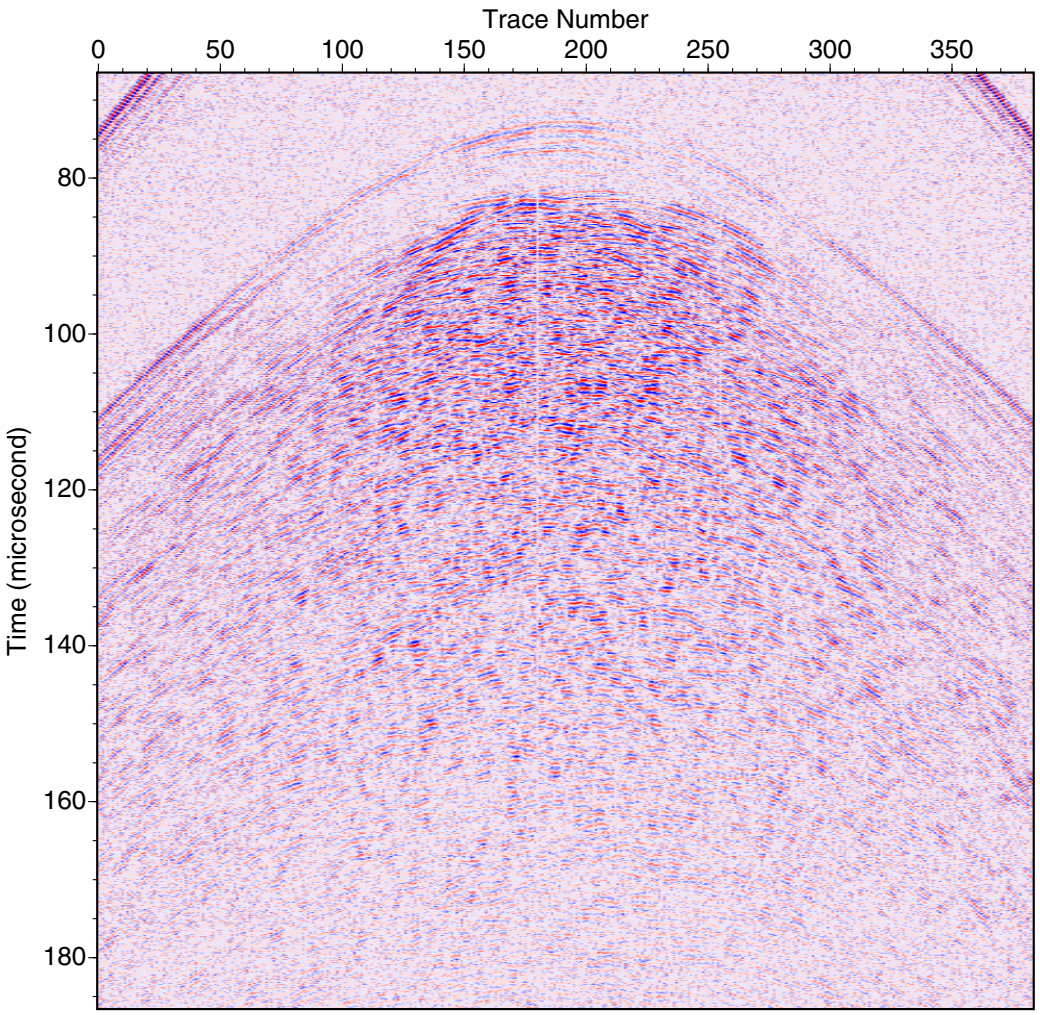

Figure 8: Virtual-source synthetic-aperture ultrasound reflection data from the breast phantom in Fig. 5(b) acquired by firing 33 transducer elements to form a virtual point source at the same location of transducer element No. 192 near the center of a transducer array. Data on two dead/weak transducer elements are shown as two vertical white strips.

measurements of the pressure, salinity and temperature of water. We use the water sound-speed c_w to compute delay times for each transducer element to emit ultrasound to form a virtual source (Fig. 6). For a virtual point source located at "A" in Fig. 6(a), the firing delay times Δt_i for the i^{th} transducer element at "B" is given by

$$\Delta t_i = \frac{\overline{\text{AB}}}{c_w}, \tag{4}$$

where $\overline{\text{AB}}$ is the distance between point "A" and point "B" in Fig. 6(a).

The virtual point sources can be formed at any spatial locations behind or in the front side of a transducer array, or on the surface of a transducer array. However, for breast imaging, it is not suitable to form virtual point sources in the front of a transducer array to avoid potential harms of heat generated by ultrasound focusing. When the location of a virtual point source is farther away from the front surface of a transducer array, the opening angle of ultrasound becomes smaller. To maximize the opening angle of ultrasound, we form virtual point sources on the surface of a transducer element array. In addition, we use a Hann window for apodization within the transducer elements to form a virtual point source.

We immerse the breast phantom in Fig. 5(b) into a warm water tank and scan the phantom using our clinical breast ultrasound tomography system in Fig. 5(a). We first acquire ultrasound reflection data with synthetic-aperture ultrasound

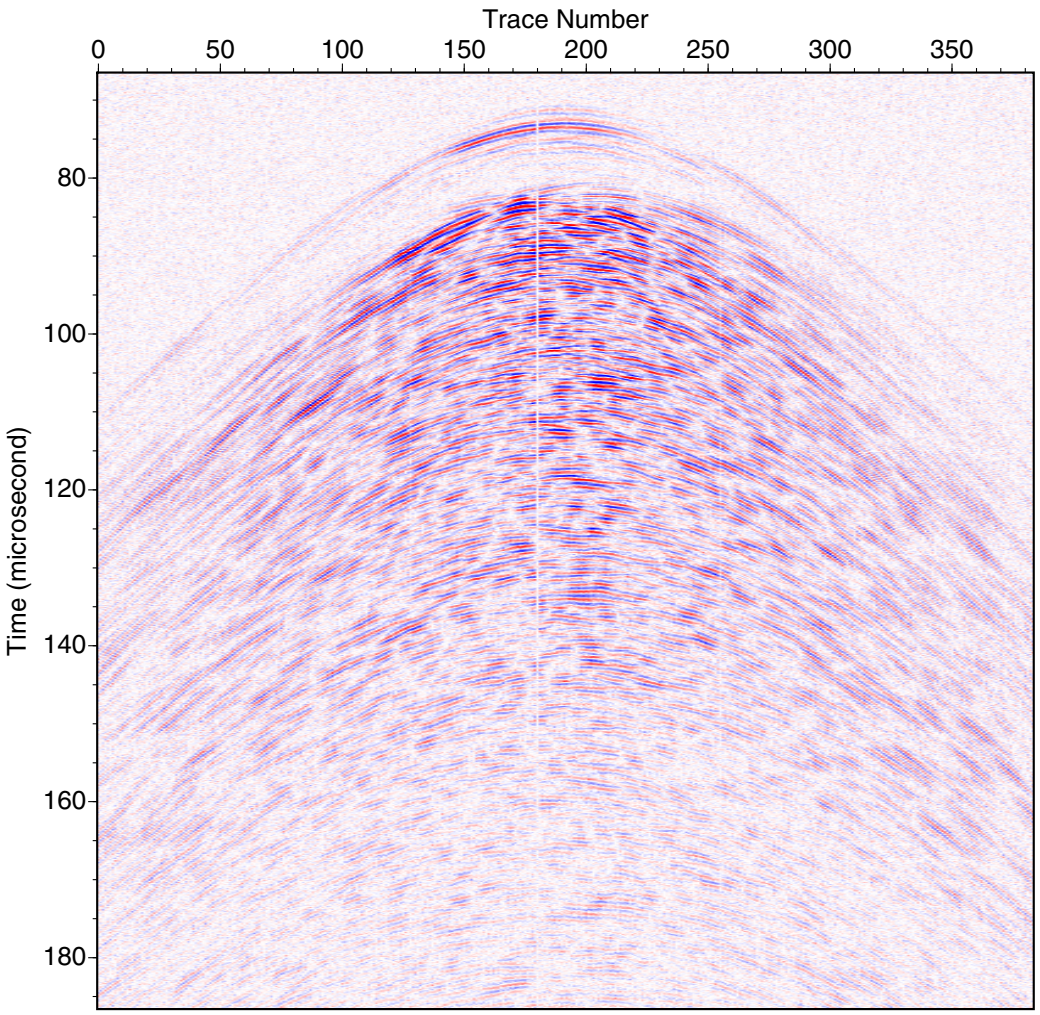

Figure 9: Numerical-virtual-source synthetic-aperture ultrasound reflection data from the breast phantom in Fig. 5(b) obtained by combining synthetic-aperture ultrasound data from 33 transmitting elements to form a numerical virtual point source at the same location of transducer element No. 192 near the center of a transducer array. Data on two dead/weak transducer elements are shown as two vertical white strips.

by firing each element sequentially using a center frequency of 1 MHz. Figure 7 displays ultrasound reflection waveforms acquired by a transducer array when firing transducer element No. 192 located near the center of a transducer array. It shows a lot of reflection signals, including reflections from the skin of the phantom, the surface of the glandular material, and other materials/inclusions embedded in the glandular material.

We then acquire ultrasound reflection data with virtual point sources by firing 33 elements to form a virtual source. We also use a center frequency of 1 MHz to fire transducer elements. We employ a Hann window with a length of 33 for apodization. Figure 8 shows virtual-source synthetic-aperture ultrasound reflection waveforms acquired by a transducer array with a virtual point source at the same location as transducer element No. 192 near the center of a transducer array. Ultrasound reflection signals in Figure 8 contain reflections from the skin of the phantom, the surface of the glandular material, and other materials embedded in the glandular material. Compared with ultrasound reflection waveforms in Fig. 7, virtual-point-source data acquisition shown in Fig. 8 enhances ultrasound reflection waveforms from the materials embedded in the glandular material. However, the background noise level in Fig. 8 is similar to that in Fig. 7. The direct ultrasound arrivals shown in the top-left and top-right corners of Fig. 8 are stronger than those in Fig. 7. This is partially because the additional cross-talk effects of the multiple firing of transmitting elements in the virtual-point-source method implemented on transducer arrays.

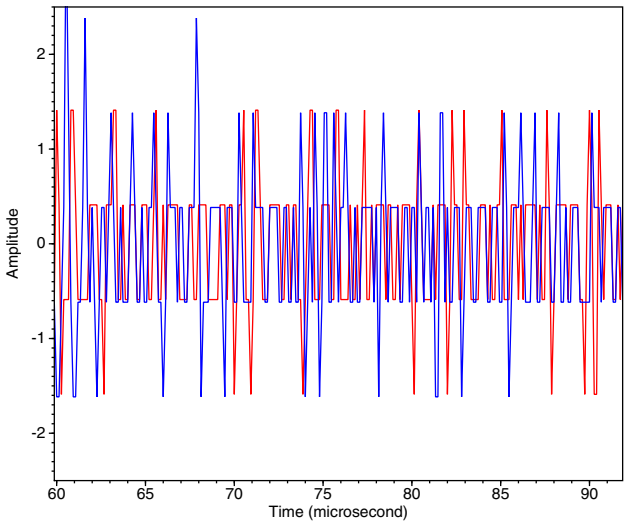

(a) Comparison between background noise of real-source synthetic-aperture ultrasound (red) and that of virtual-source synthetic-aperture ultrasound (blue)

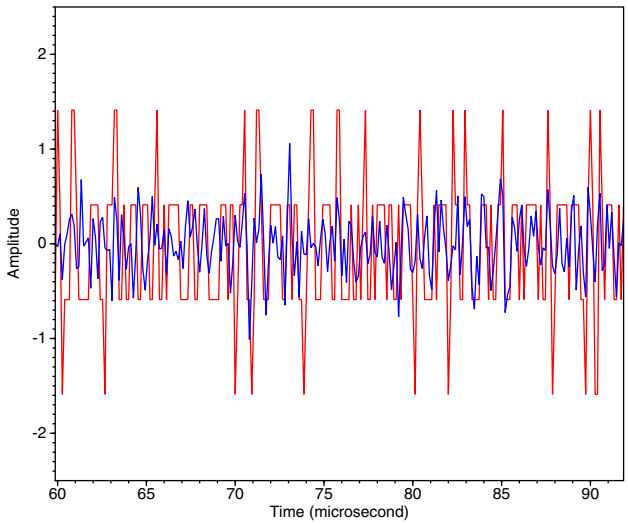

(b) Comparison between background noise of real-source synthetic-aperture ultrasound (red) and that of numerical-virtual-source synthetic-aperture ultrasound (blue)

Figure 10: Comparison among background noises of synthetic-aperture ultrasound with real sources (the red wiggle lines in both panels), virtual point sources (the blue wiggle line in a), and numerical virtual point sources (the blue wiggle line in b). Red and blue wiggle lines are ultrasound data traces from 60 to 92 microseconds at trace No. 60 in Figs. 7, 8, and 9.

3.2 Implementing virtual point sources on synthetic-aperture ultrasound data: Numerical virtual point sources

Rather than implementing virtual point sources on ultrasound transducer arrays, we develop a numerical virtual-point-source method to implement virtual point sources on synthetic-aperture ultrasound data. We combine synthetic-aperture ultrasound data d acquired by firing each transducer element sequentially to form virtual-source ultrasound waveform D for the k^{th} virtual point source located at "A" in Fig. 6(a). We refer such a virtual point source as a numerical virtual point source. The combined ultrasound data D, or the numerical-virtual-source synthetic-aperture ultrasound data, at the j^{th} transducer element is obtained using

$$D(t,j,k) = \sum_{i=1}^{M} d(t+\Delta t_i, j, i)A(i), \tag{5}$$

where i is the index for a transmitting element, M is the total number of transmitting elements for forming a numerical virtual point source, the delay time Δt_i is calculated using equation (4), and A is an apodization window with a length of M. We use a Hannn window as an apodization filter.

The advantages of our new numerical virtual-point-source method using equation (5) include:

1. One can form numerical virtual point sources located at any spatial locations after synthetic-aperture ultrasound data are acquired;
2. One can use a correct sound speed (of water) to calculate delay times;
3. One can combine data emitted from any number of transmitting elements, that is, one can choose any number of M in equation (5);
4. One can generate ultrasound data for any number of numerical virtual point sources;
5. One can store only numerical-virtual-point-source synthetic-aperture ultrasound data that are enough for imaging and tomography; and
6. The numerical virtual-point-source method implemented on acquired data eliminates the cross-talk effects of the multiple firing of transmitting elements in the virtual-point-source method implemented on transducer arrays.

When combining the synthetic-aperture ultrasound data we acquired for the breast phantom using equation (5) to obtain numerical virtual-point-source ultrasound data, we use the same delay times as those employed for forming virtual point

sources to acquire virtual-source ultrasound data in Fig. 8. We combine the synthetic-aperture ultrasound reflection data using $M = 33$ in equation (5) and a 33-point Hann window for a numerical virtual point source at the same location as transducer element No. 192. Figure 9 displays the resulting ultrasound reflection waveforms.

Fig. 9 clearly shows many coherent ultrasound waveforms reflected from the embedded materials/inclusions in the glandular material of the breast phantom, but they are not very coherent in Figs. 7 and 8. Fig. 9 also reveals several late-arrival coherent ultrasound waveforms, which are almost invisible in Figs. 7 and 8. The signal-to-noise ratio in Fig. 9 is obviously higher than those in Figs. 7 and 8. In addition, Fig. 9 does not contain the strong ultrasound signals in the top-left and top-right corners of the figure as those in Figs. 7 and 8. This could be due to the incoherent combination of ultrasound direct arrivals in our numerical virtual-point-source method.

The background noise in Fig. 9 is less significant than those in Figs. 7 and 8. Fig. 10 is a comparison of background noises among Figs. 7, 8, and 9. The background noise of virtual-source synthetic-aperture ultrasound is the same as that of real-source synthetic-aperture ultrasound (Fig. 10a). Numerical-virtual-source synthetic-aperture ultrasound significantly reduces the background noise, as shown in Fig. 10(b).

4. CONCLUSIONS

We have numerically validated that using both synthetic-aperture ultrasound transmission and reflection data in ultrasound waveform tomography significantly improves the resolution and accuracy of sound-speed reconstructions compared to when using either transmission data or reflection data alone for tomography. To enhance signal-to-noise ratios in synthetic-aperture ultrasound reflection data, we have developed a numerical virtual-point-source method to obtain high-quality ultrasound data for virtual sources located at any positions near transducer arrays. Our new method combines synthetic-aperture ultrasound data acquired by firing each transducer element sequentially. Synthetic-aperture ultrasound reflection data from a breast phantom obtained using our numerical virtual-point-source method unmask many coherent ultrasound reflection waveforms that are weak or invisible in the original data. Our numerical virtual-point-source method enables us to effectively use synthetic-aperture ultrasound reflection data together with transmission data for breast ultrasound tomography, including ultrasound bent-ray tomography and ultrasound waveform tomography.

5. ACKNOWLEDGMENTS

This work was supported by the Breast Cancer Research Program of U.S. DOD Congressionally Directed Medical Research Programs. The computation was performed using super-computers of the Institutional Computing Program of Los Alamos National Laboratory.

REFERENCES

[1] O'Donnell, M. and Thomas, L. J., "Efficient synthetic aperture imaging from a circular aperture with possible application to catheter-based imaging," *IEEE Transactions on Ultrasonics, Ferroelectrics, and Frequency Control* **39**, 366–380 (1992).

[2] Lockwood, G., Talman, J., and Brunke, S., "Real-time 3-d ultrasound imaging using sparse synthetic aperture beamforming," *IEEE Trans. Ultrason. Ferroelectr. Freq. Control* **45**, 980–988 (1998).

[3] Nikolov, S., Gammelmark, K., and Jensen, J., "Recursive ultrasound imaging," *Proceedings of the IEEE Ultrasonic Symposium* **2**, 1621–1625 (1999).

[4] Nikolov, S. I., *Synthetic aperture tissue and flow ultrasound imaging*, PhD thesis, Technical University of Denmark (2001).

[5] Huang, L., Duric, N., and Littrup, P., "Ultrasonic breast imaging using a wave-equation migration method," *Proc. SPIE* **5035**, 432–439 (2003).

[6] Jensen, J., Holm, O., Jensen, L., Bendsen, H., Nikolov, S., Tomov, B., Munk, P., Hansen, M., Salomonsen, K., Hansen, J., Gormsen, K., Pedersen, H., and Gammelmark, K., "Ultrasound research scanner for real-time synthetic aperture data acquisition," *IEEE Trans. Ultrason. Ferroelectr. Freq. Control* **52**, 881–891 (2005).

[7] Huang, L., Duric, N., and Littrup, P., "Breast imaging with time-reversed ultrasound," *Proc. SPIE* **6147**, 156–167 (2006).

[8] Jensen, J., Nikolov, S., Gammelmark, K., and Pedersen, M., "Synthetic aperture ultrasound imaging," *Ultrasonics* **44**, e5–e15 (2006).

[9] Daher, N. and Yen, J., "2-d array for 3-d ultrasound imaging using synthetic aperture techniques," *IEEE Trans. Ultrason. Ferroelectr. Freq. Control* **53**, 912–924 (2006).

[10] Simonetti, F., "Multiple scattering: The key to unravel the subwavelength world from the far-field pattern of a scattered wave," *Physical Review E* **73**, 036619–1–13 (2006).

[11] Huang, L. and Quan, Y., "Ultrasound pulse-echo imaging using the split-step Fourier propagator," *Proc. SPIE* **6513**, 651305–1–12 (2007).

[12] Simonetti, F., Huang, L., Duric, N., and Rama, O., "Imaging beyond the born approximation: An experimental investigation with an ultrasonic ring array," *Physical Review E* **76**, 036601–1–10 (2007).

[13] Simonetti, F. and Huang, L., "From beamforming to diffraction tomography," *Journal of Applied Physics* **103**, 103110–1–7 (2008).

[14] Huang, L., Hanson, K. M., Quan, Y., Li, C., and Duric, N., "Globally optimized Fourier finite-difference method for ultrasound breast imaging," *Proc. SPIE* **6920**, 692007–1–11 (2008).

[15] Andresen, H., Nikolov, S., Pedersen, M., Buckton, D., and Jensen, J., "Three-dimensional synthetic aperture focusing using a rocking convex array transducer," *IEEE Trans. Ultrason. Ferroelectr. Freq. Control* **57**, 1051–1063 (2010).

[16] Huang, L., Simonetti, F., Huthwaite, P., Rosenberg, R., and Williamson, M., "Detecting breast microcalcifications using super-resolution and wave-equation ultrasound imaging: A numerical phantom study," in [*Ultrasonic Imaging, Tomography, and Therapy*], D'hooge, J. and McAleavey, S. A., eds., *Proc. SPIE* **7629**, 762919–1–10, SPIE (2010).

[17] Nikolov, S. I., Kortbek, J., and Jensen, J. A., "Practical applications of synthetic aperture imaging," in [*Proceedings – IEEE Ultrasonics Symposium*], 350–358 (2010).

[18] Huang, L., Labyed, Y., Simonetti, F., Williamson, M., Rosenberg, R., Heintz, P., and Sandoval, D., "High-resolution imaging with a real-time synthetic aperture ultrasound system: A phantom study," in [*Ultrasonic Imaging, Tomography, and Therapy*], D'hooge, J. and Doyley, M. M., eds., *Proc. SPIE* **7968**, 79681I–1–10, SPIE (2011).

[19] Labyed, Y. and Huang, L., "Detecting small targets using windowed time-reversal MUSIC imaging: A phantom study," *International Ultrasonics Symposium Proceedings* **10.1109/ULTSYM.2011.0392**, 1579–1582 (2011).

[20] Huang, L., Labyed, Y., Lin, Y., Zhang, Z., Pohl, J., Sandoval, D., and Williamson, M., "Detection of breast microcalcifications using synthetic-aperture ultrasound," in [*Ultrasonic Imaging, Tomography, and Therapy*], D'hooge, J. and Doyley, M. M., eds., *Proc. SPIE* **8320**, 83200H–1–8, SPIE (2012).

[21] Labyed, Y. and Huang, L., "Ultrasound imaging of extended targets using a windowed time-reversal MUSIC method," in [*Ultrasonic Imaging, Tomography, and Therapy*], D'hooge, J. and Doyley, M. M., eds., *Proc. SPIE* **8320**, 832019–1–10, SPIE (2012).

[22] Labyed, Y. and Huang, L., "Ultrasound time-reversal MUSIC imaging with diffraction and attenuation compensation," *IEEE Trans. Ultrason. Ferroelectr. Freq. Control* **59**, 2186–2200 (2012).

[23] Labyed, Y. and Huang, L., "Ultrasound time-reversal MUSIC imaging of extended targets," *Ultrasound in Med. & Biol.* **38**, 2018–2030 (2012).

[24] Huang, L., Labyed, Y., Hanson, K., Sandoval, D., Pohl, J., and Williamsonb, M., "Detecting breast microcalcifications using super-resolution ultrasound imaging: A clinical study," in [*Ultrasonic Imaging, Tomography, and Therapy*], Bosch, J. G. and Doyley, M. M., eds., *Proc. SPIE* **8675**, doi: 10.1117/12.2007653, 86751O–1–10, SPIE, Bellingham, Washington (2013).

[25] Labyed, Y. and Huang, L., "Super-resolution ultrasound phase-coherent MUSIC imaging with compensation for the phase response of transducer elements," *IEEE Trans. Ultrason. Ferroelectr. Freq. Control* **60**, 1048–1060 (2013).

[26] Labyed, Y. and Huang, L., "TR-MUSIC inversion of the density and compressibility contrasts of point scatterers," *IEEE Transactions on Ultrasonics, Ferroelectrics, and Frequency Control* **61**, 16–24 (2014).

[27] Littrup, P. J., Duric, N., Azevedo, S., Chambers, D. H., Candy, J. V., Johnson, S., Auner, G., Rather, J., and Holsapple, E. T., "Computerized Ultradound Risk Evaluation (CURE) system: Development of combined transmission and reflection ultrasound with new reconstruction algorithms for breast imaging," *Acoustical Imaging* **26**, 175–182 (2002).

[28] Littrup, P., Duric, N., Leach Jr., R. R., Azevedo, S. G., Candy, J. V., Moore, T., Chambers, D. H., Mast, J. E., and Holsapple, E. T., "Characterizing tissue with acoustic parameters derived from ultrasound data," in [*Ultrasonic Imaging and Signal Proceesing*], Insana, M. and Walker, W. F., eds., *Proc. SPIE* **4687**, 354–361, SPIE, Bellingham, Washington (2002).

[29] Duric, N., Littrup, P., Holsapple, E. T., Babkin, A., Duncan, R., Kalinin, A., Pevzner, R., and Tokarev, M., "Ultrasound tomography of breast tissue," in [*Ultrasonic Imaging and Signal Processing*], Walker, W. F. and Insana, M., eds., *Proc. SPIE* **5035**, SPIE, Bellingham, Washington (2003).

[30] Duric, N., Littrup, P. J., Rama, O., and Holsapple, E. T., "Computerized ultrasound risk evaluation (CURE): First clinical results," *Acoustical Imaging* **28** (2005).

[31] Duric, N., Littrup, P., Poulo, L., Babkin, A., Pevzner, R., Holsapple, E., and Rama, O., "Detection of breast cancer with ultrasound tomography: First results with the computerized ultrasound risk evaluation (cure) prototype," *Med. Phys.* **34**, 773–785 (2007).

[32] Quan, Y. and Huang, L., "Sound-speed tomography using first-arrival transmission ultrasound for a ring array," in [*Ultrasonic Imaging and Signal Processing*], Emelianov, S. Y. and McAleavey, S. A., eds., *Proc. SPIE* **6513**, doi: 10.1117/12.709647, 651306–1–9, SPIE, Bellingham, Washington (2007).

[33] Li, C., Duric, N., and Huang, L., "Clinical breast imaging using sound-speed reconstructions of ultrasound tomography data," in [*Ultrasonic Imaging and Signal Processing*], McAleavey, S. A. and D'hooge, J., eds., *Proc. SPIE* **6920**, 692009–1–9, SPIE (2008).

[34] Li, C., Duric, N., and Huang, L., "Comparison of ultrasound attenuation tomography methods for breast imaging," in [*Ultrasonic Imaging and Signal Processing*], McAleavey, S. A. and D'hooge, J., eds., *Proc. SPIE* **6920**, 692015–1–9, SPIE (2008).

[35] Li, C., Duric, N., Littrup, P., and Huang, L., "In vivo breast sound-speed imaging with ultrasound tomography," *Untrasound in Med. & Biol.* **35**, 1615–1628 (2009).

[36] Li, C., Huang, L., Duric, N., Zhang, H., and Rowe, C., "An improved automatic time-of-flight picker for medical ultrasound tomography," *Ultrasonics* **49**, 61–72 (2009).

[37] Pratt, R. G., Huang, L., Duric, N., and Littrup, P., "Sound-speed and attenuation of the breast tissue using waveform tomography of transmission ultrasound data," in [*Physics of Medical Imaging*], Hsieh, J. and Flynn, M. J., eds., *Proc. SPIE* **6510**, 65104S–1–12, SPIE, Bellingham, Washington (2007).

[38] Lin, Y., Huang, L., and Zhang, Z., "Ultrasound waveform tomography with the total-variation regularization for detection of small breast tumors," in [*Ultrasonic Imaging, Tomography, and Therapy*], Bosch, J. G. and Doyley, M. M., eds., *Proc. SPIE* **8320**, doi: 10.1117/12.910765, 832002–1–9, SPIE, Bellingham, Washington (2012).

[39] Zhang, Z., Huang, L., and Lin, Y., "Efficient implementation of ultrasound waveform tomography using source encoding," in [*Ultrasonic Imaging, Tomography, and Therapy*], Bosch, J. G. and Doyley, M. M., eds., *Proc. SPIE* **8320**, doi: 10.1117/12.910969, 832003–1–10, SPIE, Bellingham, Washington (2012).

[40] Lin, Y. and Huang, L., "Ultrasound waveform tomography with a modified total-variation regularization scheme," in [*Ultrasonic Imaging, Tomography, and Therapy*], Bosch, J. G. and Doyley, M. M., eds., *Proc. SPIE* **8675**, doi: 10.1117/12.2007650, 86751F–1–9, SPIE, Bellingham, Washington (2013).

[41] Zhang, Z. and Huang, L., "Ultrasound waveform tomography using wave-energy-based preconditioning," in [*Ultrasonic Imaging, Tomography, and Therapy*], Bosch, J. G. and Doyley, M. M., eds., *Proc. SPIE* **8675**, doi: 10.1117/12.2007659, 86751G–1–10, SPIE, Bellingham, Washington (2013).

[42] Frazier, C. H. and O'Brien Jr., W. D., "Synthetic aperture techniques with a virtual source element," *IEEE Trans. Ultrason. Ferroelectr. Freq. Control* **45**, 196–207 (1998).

[43] Bae, M.-H. and Joeng, M.-K., "A study of synthetic-aperture imaging with virtual source elements in B-mode ultrasound imaging systems," *IEEE Transactions on Ultrasonics, Ferroelectrics, and Frequency Control* **47**, 1510–1519 (2000).

[44] Nikolov, S. I. and Jensen, J. A., "Virtual ultrasound sources in high-resolution ultrasound imaging," in [*Ultrasonic Imaging and Signal Processing*], Insana, M. F. and Walker, W. F., eds., *Proc. SPIE* **4687**, 395–405, SPIE, Bellingham, Washington (2002).

[45] Jatoi, I., Hilsenbeck, S. G., and andand C. Kent Osborne, G. M. C., "Significance of axillary lymph node metastasis in primary breast cancer," *Journal of Clinical Oncology* **17**, 2334–2340 (1999).